Polymer 51 (2010) 3978–3988

Contents lists available at ScienceDirect

Polymer

journal homepage: www.elsevier.com/locate/polymer

Microphase separation in copolymers of hydrophilic PEG blocks and hydrophobic tyrosine-derived segments using simultaneous SAXS/WAXS/DSC

N.S. Murthy [a], W. Wang [b], J. Kohn [a,*]

[a] New Jersey Center for Biomaterials, Rutgers University, Piscataway, NJ 08854, USA
[b] Physics Department, University of Vermont, Burlington, VT 05405, USA

ARTICLE INFO

Article history:
Received 1 April 2010
Received in revised form
10 June 2010
Accepted 13 June 2010
Available online 18 June 2010

Keywords:
PEG copolymers
Hydration
Phase separation

ABSTRACT

Hydration- and temperature-induced microphase separations were investigated by simultaneous small- and wide-angle X-ray scattering (SAXS and WAXS) and differential scanning calorimetry (DSC) in a family of copolymers in which hydrophilic poly(ethylene glycol) (PEG) blocks are inserted randomly into a hydrophobic polymer made of either desaminotyrosyl-tyrosine ethyl ester (DTE) or iodinated I_2DTE segments. Iodination of the tyrosine rings in I_2DTE increased the X-ray contrast between the hydrophobic and hydrophilic segments in addition to facilitating the study of the effect of iodination on microphase separation. The formation of phase-separated, hydrated PEG domains is of considerable significance as it profoundly affects the polymer properties. The copolymers of DTE (or I_2DTE) and PEG are a useful model system, and the findings presented here may be applicable to other PEG-containing random copolymers. In copolymers of PEG and DTE and I_2DTE, the presence of PEG depressed the glass transition temperature (T_g) of the copolymer relative to the homopolymer, poly(DTE carbonate), and the DTE/I_2DTE segments hindered the crystallization of the PEG segments. In the dry state, at large PEG fractions (>70 vol%), the PEG domains self-assembled into an ordered structure with 14–18 nm distance between the domains. These domains gave rise to a SAXS peak at all temperatures in the iodinated polymers, but only above the T_g in non-iodinated polymers, due to the unexpected contrast-match between the crystalline PEG domains and the glassy DTE segments. Irrespective of whether PEG was crystalline or not, immersion of these copolymers in water resulted in the formation of hydrated PEG domains that were 10–20 nm apart. Since both water and the polymer chains must be mobile for the phase separation to occur, the PEG domains disappeared when the water froze, and reappeared as the ice began to melt. This transformation was reversible, and showed hysteresis as did the melting of ice and freezing of the water incorporated into the polymer. PEG–water complexes and PEG–water eutectics were observed in WAXS and DSC scans, respectively.

1. Introduction

Low molecular weight poly(ethylene oxide), commonly called poly(ethylene glycol) (PEG), is a water soluble polymer that lacks toxicity and immunogenicity and is rapidly cleared from the body. PEG containing copolymers have been investigated in numerous biomedical applications, e.g., improving blood compatibility [1], reducing immunogenicity [2], and reducing protein adsorption and cell attachment [3]. Polymer solubility can be modified by incorporating PEG segments into water-insoluble polymers. The stability and mechanical properties of a polymer can be modified by combining soft PEG segments with various hard segments as illustrated by copolymers of PEG and lactide [4]. However, the incorporation of hydrophilic PEG segments into a hydrophobic polymer backbone has a major drawback: the properties of the resulting copolymers are affected by the morphological changes that occur with changes in temperature and moisture. Control over performance of the copolymer requires a fundamental understanding of the polymer's complex phase behavior.

The influence of PEG depends on whether the polymer is a blend [5,6], a graft [1,7], a diblock [8–10] or a segmented block [11] copolymer. Segmented block copolymers with PEG as one of the blocks have been studied in aqueous solution [12–14], gel [15], and in the solid phase [10,16,17]. There are numerous papers [18–22] and books [23–27] on copolymers that deal with phase behavior in di- and tri-block copolymers. However, the temperature- and hydration-induced microphase separation in multi-block copolymers is a complex process that has not been studied in sufficient detail. A knowledge of this process is important for understanding

* Corresponding author. Tel.: +1 732 445 3888.
E-mail address: kohn@biology.rutgers.edu (J. Kohn).

0032-3861/$ – see front matter © 2010 Elsevier Ltd. All rights reserved.
doi:10.1016/j.polymer.2010.06.024

the results of the hydrolytic degradation studies in biomedically relevant copolymers [28–32] that are often designed to be biodegradable. The process of degradation is expected to begin with the hydration of the PEG segments that results in morphological changes. These changes may play an important role in determining other material properties such as mechanical behavior, protein adsorption, cellular response, and drug release. Mechanisms of hydration are not understood well enough to be able to predict the performance of a degrading biomedical implant over time.

Here we study a model system of polymers consisting of PEG as the hydrophilic block and desaminotyrosyl-tyrosine ethyl ester (DTE) as the hydrophobic segments to elucidate the general role and characteristics of PEG in random segmented block copolymers. The polymers in this family are biodegradable, and their mechanical properties, water uptake, biocompatibility and resorption characteristics can be precisely controlled by varying the polymer composition. Therefore, they are good candidates for a variety of biomedical applications including drug delivery devices and orthopedic implants. This family of random segmented block copolymers was made by inserting PEG blocks of different molecular weights (PEG_{nk}, where nk is the molecular weight of PEG in 1000 Da) randomly into the poly(DTE carbonate) main chain (Fig. 1) [33–35]. Iodinated versions of these polymers [36], poly(I_2DTE carbonate), in which the desaminotyrosine rings have been iodinated, provide the X-ray contrast between the DTE segments and PEG blocks. They also provide an opportunity to study the effect of iodination on the morphology of copolymers. Our results are of wider significance, for they are relevant to other polymers with at least one hydrophilic and one hydrophobic block.

This study extends our recent small-angle neutron scattering (SANS) study [37] in which water was found to be unevenly distributed in the polymer, existing as isolated ~10 nm domains in poly(DTE-*co*-PEG_{1k} carbonate)s at low molar fraction of PEG_{1k} (5%) and as clusters of domains at higher PEG_{1k} molar fractions (20%). Small- and wide-angle X-ray scattering (SAXS and WAXS) results are used to determine whether the phase-separated PEG-rich domains cause water to accumulate into domains, or if the PEG-rich domains evolve during hydration. Evolution of the scattering patterns as a function of temperature during differential scanning calorimetry (DSC) scans will be analyzed to understand the hydration and phase behavior in copolymers with different PEG block sizes and PEG fractions. Furthermore, the effects of the stiffness (chain mobility) and the hydrophobicity of the main chain on the phase behavior of the polymers are explored by using polymers with and without iodinated desaminotyrosine rings.

2. Materials and methods

The set of polymers studied includes six polymers of the general composition poly(DTE-*co*-*x*% PEG_{nk} carbonate)s and six polymers in which the desaminotyrosine ring was doubly iodinated, poly(I_2DTE-*co*-*x*% PEG_{nk} carbonate)s (Table 1).

Poly(L-lactic acid), PLLA, was purchased from Boerhringer Ingelheim (Resomer L 207, lot No. 232128). All other polymers were prepared and characterized by previously reported methods [35]. Molecular weight (M_w) was determined by gel permeation chromatography (GPC). Polymers were measured with two PL-gel columns with pore sizes 103–105 Å (Polymer Labs) using tetrahydrofuran (THF) as a mobile phase (Perkin–Elmer, Waters 410 RI detector), at a flow rate of 1 mL/min. M_w was determined relative to polystyrene standards.

Films of thickness ~200 μm were compression-molded using a Carver press at $T_g + 75$ °C and 15,000 lbf. The mold was allowed to gradually cool to room temperature and the film was removed from the mold.

DSC data were obtained on a Mettler DC 823 unit typically at heating and cooling rates of 10 °C/min using samples of ~10 mg. T_g was calculated from the intersection point of a horizontal line at half step height and the inflectional tangent; step-height is the change in the specific heat between the onset and endpoint of the glass relaxation (ASTM midpoint method). Dry T_g was determined from the re-heat scan so as to eliminate the effects of the enthalpic relaxation peak and the residual solvents often seen during the first heating. Wet T_g was determined from the first heat to ensure that water was in the sample.

Equilibrium water uptake (EWU) values were obtained from thermogravimetric analysis (TGA) data using the expression

$$\text{EWU}\ (\%) = \frac{\left(M_{\text{wet}} - M_{\text{dry}}\right)}{M_{\text{wet}}} 100 \quad (1)$$

where M_{wet} and M_{dry} are the weights of the polymer at 23 and 150 °C as they are heated in the TGA pan.

For X-ray scattering measurements, films of ~5 mm diameter were hydrated by immersing them in 5 ml phosphate buffered saline (PBS) (Sigma) at ambient temperatures. Low water-uptake materials (PEG < 25 wt%, which reach EWU at ~20 h) were immersed for ~24 h and high water-uptake materials (PEG > 25 vol%, which reach EWU in ~1 h) were immersed for ~6 h.

X-ray scattering measurements were carried out in the 5ID-D enclosure of DND-CAT at the Advanced Photon Source at the Argonne National Laboratory (Argonne, IL). Simultaneous SAXS/WAXS/DSC data were acquired in transmission mode from samples (6–9 mg) mounted in high-pressure pans on a Linkam® CI93 DSC as the samples were heated at 10 °C/min. A temperature range from −80 to 150 °C was available; the actual range for individual scans was typically from −30 °C below to 30 °C above T_g. The X-ray beam (0.10332 nm wavelength) from a Si- (111) double crystal monochromator was collimated with three sets of slits to about 0.2 × 0.2 mm. WAXS data were collected on a 100 × 200 mm

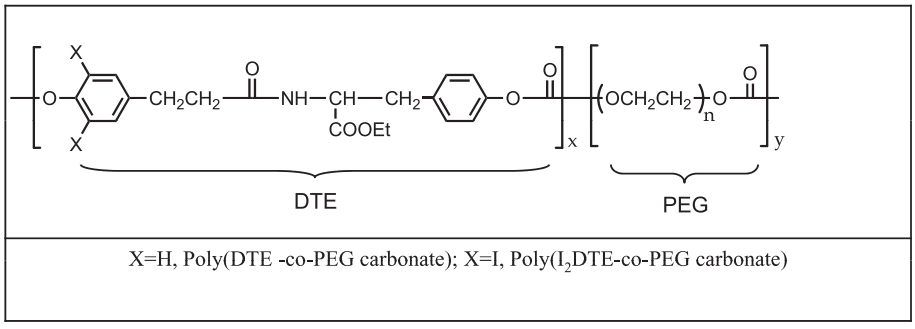

Fig. 1. Basic structural units of the family of model polymers used in this investigation.

Table 1
Relevant parameters of poly(DTE-*co*-PEG carbonate) polymers (EWU – Equilibrium water uptake).

Non-iodinated polymers							Iodinated polymers						
PEG content			Mol. wt.	EWU	T_g (°C)		PEG content			Mol. wt.	EWU	T_g (°C)	
Mol%	Wt%	Vol%	(kDa)	wt%	Dry	Wet	Mol%	Wt%	Vol%	(kDa)	wt%	Dry	Wet
0%	0	0		3.0	91.7	64.0	0%	0.0	0.0	219	1.5	135.5	113.2
5% PEG_{1k}	12.8	14.7	198	5.3	64.4	33.1	5% PEG_{1k}	9.8	15.9	57	2.7	88.8	43.0
8% PEG_{1k}	19.6	22.1	78	10.4	46.0	25.7	8% PEG_{1k}	12.5	19.9	89	6.2	77.5	44.7
10% PEG_{1k}	23.7	26.7	186	12.5	40.4	25.4	10% PEG_{1k}	15.4	24.1	34	12.5	49.4	21.6
20% PEG_{1k}	41.2	45.0	75	42.3	5.0		24% PEG_{1k}	34.1	47.4	45	18.9	9.1	
15% PEG_{2k}	49.7	53.6	140	63.4	−24.7		15% PEG_{2k}	36.7	50.2	113	29.3	0.42	
30% PEG_{2k}	70.6	73.7	226	84.8	−43.5		30% PEG_{2k}	58.5	71.0	129	62.2	−31.1	
							8% PEG_{8k}	53.3	66.5	59	67.4	−38.3	
0.71% PEG_{35k}	41.2	45.0	185	55.8	−8								

Parameters for PLLA: T_g (Dry) = 66 °C; T_m = 177 °C; EWU 0.5% [55].
T_m of PEG in the copolymers: 39 °C for PEG (2 k); 49 °C for PEG (8 k) and 56 °C PEG (35 k).

dual chip Roper® CCD camera with a sample to detector distance of 230 mm. Dark frame, distortion, and flat-field corrections were performed with FIT2D [38]. SAXS data were simultaneously collected on a 100 × 100 mm Roper camera with a sample to detector distance of 2897 mm. X-ray scattering data were obtained with 2–20 s exposures depending on the sample.

2D X-ray scattering (both SAXS and WAXS) images were processed to obtain 1D data that will be presented in this paper in the form of $I(q)$ as a function of the scattering vector q; $I(q)$ is the radially averaged intensity at each value q; $q = 4\pi\sin\theta/\lambda$, where 2θ is the scattering angle and λ is the wavelength. Using Bragg's Law, d-spacing (d) was obtained from $q_{max}=2\pi/d$, where q_{max} is the q-value of the peak in I(q).

3. Results and discussion

The general structure of the polymer is shown in Fig. 1. The polymers poly(DTE-*co*-*x*% PEG_{nk} carbonate) and poly(I_2DTE-*co*-*x*% PEG_{nk} carbonate) will be identified as *x*% PEG_{nk} DTE or *x*% PEG_{nk} I_2DTE, respectively. In this nomenclature, *x*% is the mol% of PEG and nk is the molecular weight of PEG in 1000 Da. The PEG content will be given in wt% while discussing water uptake and in vol% while discussing the phase behavior. The volume fractions were calculated using the following densities for the various phases: poly(DTE carbonate) – 1.324 g/cm^3; poly(I_2 DTE carbonate) – 1.952 g/cm^3 (both from modeling X-ray reflectometry data; Aamer/NIST, private communication; these are probably the upper limits; since these polymers are amorphous, their densities are sensitive to processing conditions, and we have observed densities lower than these values); and PEG −1.124 g/cm^3 [39]. Table 1 summarizes the relevant characteristics and properties of the polymers.

There are two variables in the polymers chosen for this study: the PEG content and the iodination of the DTE segments. The polymers chosen do not cover a range of PEG molecular weights large enough to study in detail the effects of PEG block size. Iodine provides the contrast between DTE segments and PEG blocks that is useful in studying the phase behavior. Iodine also changes the hydrophobicity of the polymer, the chain stiffness and the packing density. The resulting effect of iodine, based on the data in Table 1, is twofold: it increases the chain stiffness or reduces the chain mobility (increased T_g), and it limits the water uptake. Wet T_gs could be measured only when these values were above 0 °C, such that the glass transition did not overlap the melting of ice or the freezing of water. In some wet samples (e.g., 20% PEG_{1k} DTE and 15% PEG_{2k} DTE), the small changes in the specific heat at T_g were masked by the large changes in heat flow that accompanied the melting of ice and crystallization of water. Wet T_gs in some other samples (e.g., 30%PEG_{2k} I2DTE and 8% PEG_{8k} I2DTE) were below the temperature range of our equipment.

WAXS scans plotted in Fig. 2a show that even though the iodine atoms are bulky, the interchain distance calculated from the peak maximum of the amorphous halo decreases from 0.465 to 0.422 nm (peak shifts to higher q values) when the desaminotyrosine rings are iodinated. This counter-intuitive observation suggests that the restricted rotational motion of the chains with iodinated desaminotyrosine rings results in closer packing of the chains. This is consistent with the higher T_g in the iodinated polymers (Table 1) and with the previously reported increased modulus [40]. Fig. 2b shows that the interchain spacing of the non-iodinated polymer decreases with the increasing PEG content and approaches that of the iodinated polymer, which remains essentially unchanged.

3.1. Crystallization of PEG segments in dry samples

DSC and X-ray data have shown that in multi-block copolymers of PEG with PLA, depending on the size of the two blocks, amorphous matrices and monophasic crystalline phases in which either or both PLA and PEG are crystalline can be formed [4]. Also, in graft

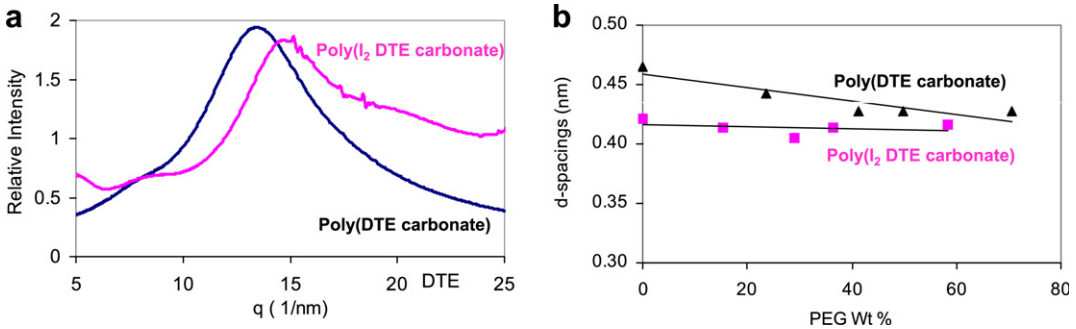

Fig. 2. (a) WAXS scans of dry samples of iodinated and non-iodinated DTE homopolymers room temperature. (b) Changes in *d*-spacings of the main polymer peak in iodinated (squares) and non-iodinated (triangles) polymers as a function of PEG content.

copolymers, with PEG block lengths similar to those used here, PEG segments were found to phase separate at all concentrations and block sizes, even in the melt, and crystallize upon cooling [41]. But, the PEG segments crystallized in only four of the polymers listed in Table 1, those with more than ~50 vol% of PEG, and 40%PEG_{1k} DTE (68.6 vol% PEG), which is not included in the table. Additionally, PEG was crystalline in the 0.71% PEG_{35k} polymer with 45 vol% PEG, most likely because of its high molecular weight. PEG crystalline peaks can be seen in the WAXS scans (Fig. 3a and b) and in the melting endotherm at ~40 °C in the DSC scans (Fig. 4). In general, DTE segments appear to inhibit the crystallization of PEG blocks when their volume fraction is small (<50%; 15% PEG_{2k} I_2DTE with 50.2% was the last polymer in which PEG was not crystalline) especially when the block sizes are <35 kDa. At larger PEG fractions, the PEG blocks crystallize even when randomly distributed along the main chain.

As in other copolymers [4,41], the melting point of PEG crystals in our copolymers that were present during the first heat was depressed from its homopolymer value of 54 °C to ~40 °C. But the PEG segments did not recrystallize during cooling in any of our polymers (Fig. 4), even when cooled at 1 °C/min. The PEG blocks in polymers such as 15 and 30% PEG_{1k} DTE and 30% PEG_{1k} I_2DTE should have crystallized during cooling at ~20 °C below T_m as observed in other copolymers [7]. PEG blocks did crystallize when the samples were aged (~3 days). This suggests that once PEG is molten, the interactions between the PEG and DTE or I2DTE segments inhibit its recrystallization during cooling. As a result, there are no PEG crystals to melt during reheat.

PEG segments crystallized during heating in two of the compositions that were examined here, 30% PEG_{2k} DTE (Fig. 4a) and 8% PEG_{8k} I_2DTE (scan not shown). Relative values of the T_g of the polymer and the crystallization temperature of PEG upon heating (T_{ch}) appear to determine the crystallization behavior of PEG. The T_g and T_{ch} values for 30% PEG_{2k} DTE are −43.5 and −9.3 °C, respectively, and for 8% PEG_{8k} I_2DTE, they are −38.3 and 3.3 °C, respectively. These and other similar data suggest that for PEG to crystallize in our polymers, T_{ch} needs to be far above the T_g, in this particular case by 30 °C. This explains the presence of PEG crystals in the 15% PEG_{2k} DTE (T_g = −24.7 °C, and T_{ch} = −9.3 °C) but not in the 15% PEG_{2k} I_2DTE (T_g = 0.4 °C, and T_{ch} = −9.3 °C). Greater rigidity of the I_2DTE backbone raises the T_g of the polymer high enough to prevent the crystallization of PEG in the 15% PEG_{2k} I_2DTE polymer during both heating and cooling.

Just as the DTE segments inhibit the crystallization of PEG during the first heat, PEG blocks depress the T_g of the DTE segments (Table 1).

3.2. Self-assembled PEG domains in dry samples

Crystallization of PEG segments discussed in the previous section is indicative of the phase separation at large (>50 vol%) PEG contents in these families of polymers. When the phase-separated PEG domains are far apart, irrespective of whether they are crystalline or not, they give rise to diffuse low-angle scattering in SAXS patterns. This feature was observed in all dry polymers with PEG content <50 vol%. However, a SAXS interference peak was present in polymers with PEG content >70 vol% (Fig. 3c and d). This peak is not due to PEG lamellae but due to PEG domains organizing into meso-scale structures: there were instances (e.g., 15 and 30% PEG_{2k} DTE polymers) in which PEG was crystalline as seen in WAXS (30% PEG_{2k} DTE polymer shown in Fig. 3a), yet a SAXS peak was not present (e.g., −80 °C scan of 30% PEG_{2k}; Fig. 3c). A distribution of PEG block lengths and the random distribution of these blocks along the DTE chain most likely prevent PEG from forming lamellae. The PEG crystals in these polymers form by segregation and not by chain folding. Furthermore, absence of a SAXS peak in the 0.71% PEG_{35k} (45 vol% PEG) polymer despite PEG being crystalline (scans not shown) indicates that it is the total PEG content and not the block size that determines whether or not PEG forms ordered structures.

Highly ordered structures can be obtained in di- and tri-block copolymers with PEG as one of the blocks [24,27,42]. Our data show that such meso-scale structures occur in our random segmented

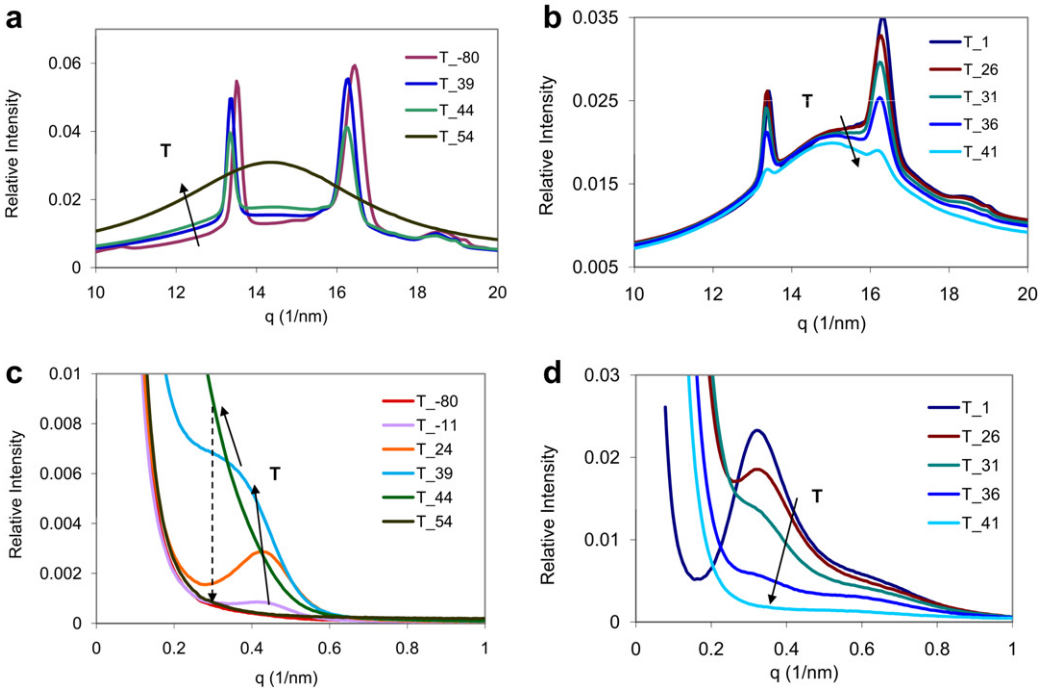

Fig. 3. X-ray scattering curves of dry samples at different temperatures obtained during first heating in a simultaneous DSC measurement. (a) WAXS scans of 30% PEG_{2k} DTE. (b) WAXS scans of 30% PEG_{2k} I_2DTE. (c) SAXS scans of 30% PEG_{2k} DTE. (d) SAXS scans of 30% PEG_{2k} I_2DTE.

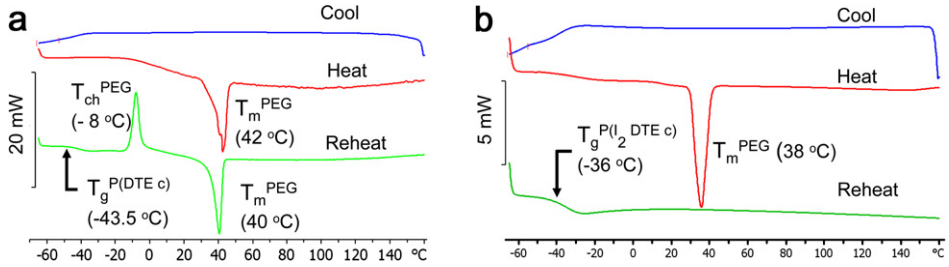

Fig. 4. DSC scans (heat, cool and reheat) of samples used for Fig. 3. (a) 30% PEG_{2k} DTE showing cold crystallization seen during reheating. (b) 30% PEG_{2k} I_2DTE, showing absence of PEG crystallization.

copolymers with >70 vol% PEG. This is readily seen in 30% PEG_{2k} I_2DTE (Fig. 3d) and 8% PEG_{8k} I_2DTE (data not shown) which showed a SAXS peak ($d \sim 18$ nm) at all temperatures at which PEG was crystalline (Fig. 3b). In contrast, the behavior of the corresponding non-iodinated polymer was more intriguing (Fig. 3c). In this polymer, an interference SAXS peak began to develop at −60 °C ($d \sim 14$ nm), continued to increase in intensity up to 39 °C, transformed into an intense central diffuse scattering upon the onset of melting of PEG (as seen in the decrease in the intensity of the WAXS crystalline peaks at 44 °C), and disappeared at 54 °C when PEG was completely molten (as seen by the disappearance of the PEG crystalline peaks into an amorphous halo), Fig. 3a and c. These differences in the temperature-dependent SAXS features between the iodinated and the non-iodinated polymers can be attributed to the differences in the electron densities of the polycarbonate matrices in the two polymers. The electron densities of the crystalline PEG domains, DTE segments and I_2DTE segments are 406, 412, and 566 nm^{-3}, respectively. Thus, there will be sufficient electron density contrast between the PEG domains and the polymer matrix on both sides of the T_g in the iodinated polymer. But the contrast is insufficient in the non-iodinated polymer, where the contrast is small between the PEG crystals and DTE segments below the T_g of the polymer. However, the contrast increases with temperature above the T_g, for the specific volume of the DTE segments increases substantially. This gives rise to the observed gradual increase in the intensity of the SAXS peak. The SAXS peak disappears when PEG is molten, as the PEG segments form structured domains and become uniformly distributed in the DTE matrix. Most importantly, when the sample was cycled repeatedly between −80 and 20 °C, without melting the PEG crystallites, the SAXS peak disappeared at −80 °C and reappeared at 20 °C. This shows that the interference peak is not due to PEG lamellae but to the ordering of the PEG domains in the DTE matrix. Similar, but less pronounced, behavior was observed, in the 15% PEG_{2k} DTE polymer.

The SAXS interference peak disappeared in all polymers when PEG was molten at 53 °C indicating that, unlike graft copolymers [41], these polymers are homogeneous in the melt (Fig. 3c and d). PEG does not crystallize upon cooling most likely because of the strong PEG–DTE interactions in the molecularly dispersed state in the melt.

3.3. Effect of hydration on interchain interactions

The PEG crystalline peaks that were present in some of the dry samples (Fig. 3a and b) disappeared when the polymers were exposed to water indicating disruption of the PEG domains. WAXS scans of frozen, hydrated samples (Fig. 5a) show crystalline peaks of ice overlaid on an amorphous halo at $q \sim 14$ nm^{-1} from the DTE segments in the polymer. The interchain d-spacings observed in the hydrated state, measured from this amorphous halo, were similar to those of the dry polymers (Figs. 5c and 2b).

There were no changes in scattering profiles in the low-PEG polymers when they were heated up to 80 °C, the highest temperature used. However, there were large changes in the scattering profiles of polymers with >10% PEG soon after the melting of ice (12 °C): The crystalline peaks of ice (formed at −20 °C during cooling) transform into an intense shoulder at $q = 19$ nm^{-1} (Fig. 5a and b) and can be seen as a distinct peak in the scans from polymers with high PEG fractions (water contents). With the increase in water content, the intensity of this 19 nm^{-1} halo increases and its d-spacing decreases (Fig. 5c). The d-spacing of this peak is ~0.35 nm, the smallest value of 0.329 nm obtained from polymers with highest water (PEG) is larger than the 0.313–0.324 nm in liquid water [43]. Therefore, this peak is due to hydrated PEG and not to liquid water. Such PEG–water complexes give rise to complex thermal transitions observed in DSC scans (Sections 3.6 and 3.7).

3.4. Phase behavior in hydrated samples

In semicrystalline polymers with lamellar structure, such as PLLA, water preferentially diffuses into the amorphous regions, alters the contrast [44], and thereby changes the SAXS intensity profile. PEG shows similar behavior, but absorbs considerably more water than PLLA, swells upon hydration and eventually dissolves. The segmented block copolymers discussed here are different from these two polymers: they are stiff at low PEG contents, deform plastically to high strain at intermediate values, become gels at even higher PEG contents, and dissolve at PEG content >70 vol%. Note that in dry polymers, PEG phase separates when present at >70 vol%.

All polymers with PEG content >10 wt% (~3 wt% water), irrespective of whether or not they had any SAXS peaks when dry, showed a SAXS interference peak when they were wet (Fig. 6a). These peaks were similar to the interference peaks seen in some of the dry samples (>70 vol% PEG; Fig. 3d). The absence of a SAXS peak in polymers with <15 vol% PEG, and its presence in all other polymers, is corroborated by SANS data [37]. This suggests that PEG segments at low concentrations are homogeneously distributed in the polymer, and the peaks in hydrated samples with >15 vol% PEG are due to the formation of PEG-rich domains within which PEG chains are hydrogen-bonded to the water molecules. PEG chains become more mobile when hydrated, and this leads to the phase separation of the hydrophilic PEG-rich domains and the hydrophobic DTE segments. This hydration-induced phase separation gives rise to the ~0.4 nm^{-1} ($d \sim 15$ nm) peak in SANS. The SAXS peak was more intense in the iodinated polymers than in the non-iodinated ones, confirming that the interference peak is due to the segregation of the DTE segments and the PEG blocks. Data in Table 2 show that the d-spacings of the hydrated domains do not increase with the amount of PEG at a fixed block size; in fact, in some instances it decreases. This suggests that as the PEG content was

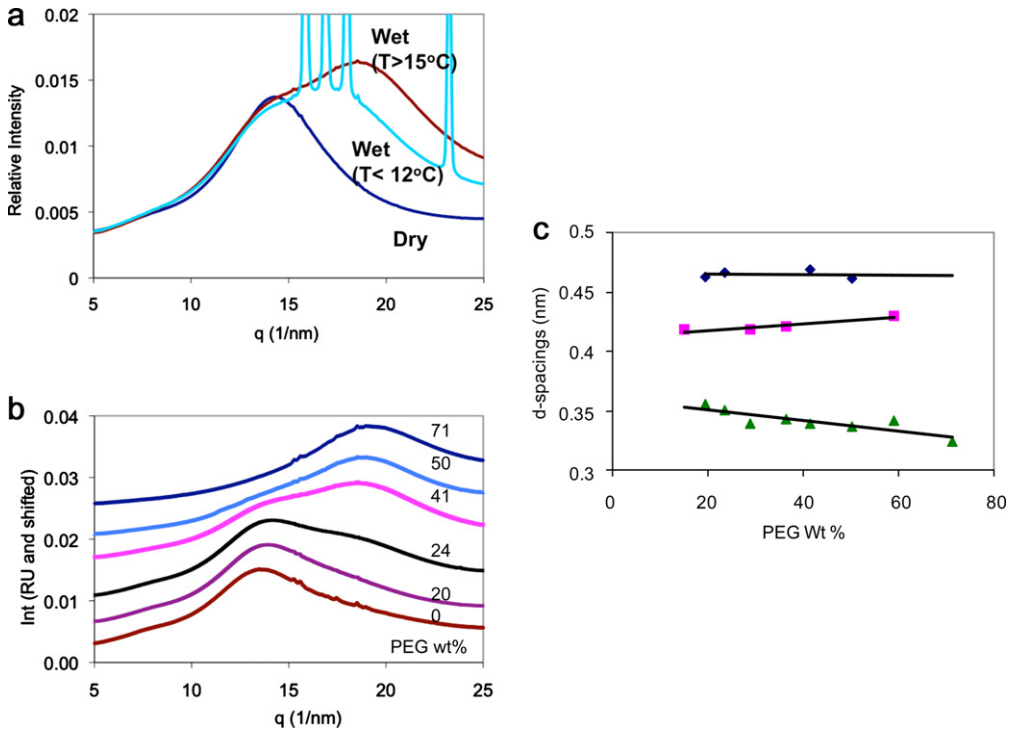

Fig. 5. (a) WAXS scans of wet samples (20% PEG_{1k}), highlighting the onset of PEG–water peak after the melting of ice. The wet scans shown in the figure for $T < 12$ °C and $T > 15$ °C were obtained at 2 and 25 °C, respectively; the dry scan was obtained at 25 °C. (b) WAXS data showing the PEG–water peak at different PEG contents. (c) Changes at room temperature in the *d*-spacing between the DTE segments (circles), I_2DTE segments (squares) and PEG–water complexes (triangles) at different PEG (water) contents.

increased, the structure evolved not by growth, but by nucleation of new PEG domains.

The SAXS inter-domain interference peak in samples with high PEG content (large water uptake) was very weak when water was frozen and became intense as the ice melted. This change was reversible (Fig. 6a). In contrast, this peak in low-PEG (low water uptake) polymers was intense even when water was frozen (Fig. 6b; 12.5 wt% water) and changed little when ice melted, as can be seen by comparing the scans at −68 and 36 °C. The difference in this behavior is most likely due to the state of water (free, bound, freezing and non-freezing), which depends on the PEG content in these polymers (see Section 3.6). It could be that mobility of the water molecules is a prerequisite for the formation of PEG-rich domains in high-PEG polymers in which PEG is the matrix but not in the low-PEG polymers in which DTE is the matrix. In all instances, the SAXS peak disappeared at ~60 °C. In SAXS scans obtained during cooling, the same peak reappeared in high-PEG polymers, but a different peak appeared in low-PEG polymers (see Section 3.7).

The segregation of the hydrophilic and hydrophobic domains influences the diffusion-dependent polymer properties, such as drug release and degradation. For instance, hydrated domains of 10 nm-size are most likely the precursors of the interconnected network of high diffusivity channels at larger length scales of 50–100 nm observed in transmission electron microscopy (TEM) [45].

3.5. Model for the hydrated domains

Homogeneous distribution of PEG blocks in the dry polymer, as suggested by the absence of a peak in SAXS scans, is schematically illustrated in Fig. 7a. A model for the phase separated structure in hydrated copolymers, as suggested by the presence of an interference peak in SAXS scans, is shown in Fig. 7b. The size of a globular PEG_{1k} block is <1 nm, based on the radius of gyration of 1.5 nm for

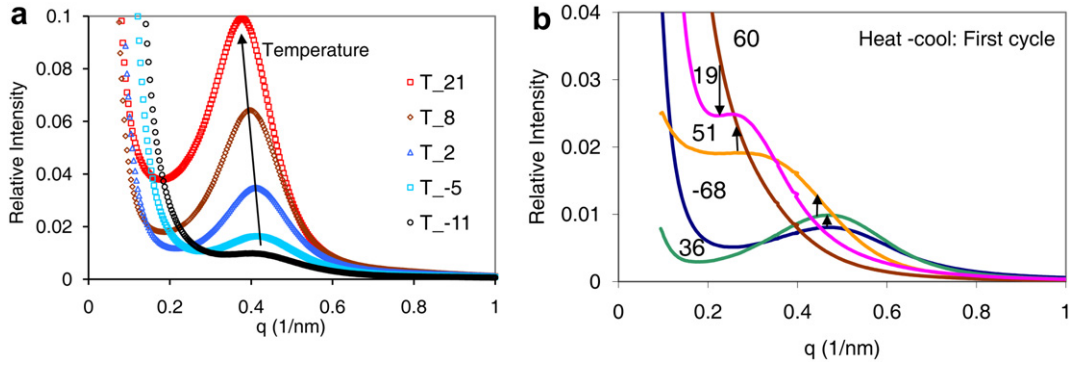

Fig. 6. SAXS data showing the evolution of the SAXS peak following the melting of ice. (a) 20% PEG_{1k} DTE; these changes are reversible. (b) 10% PEG_{1k} DTE; these changes are not reversible (see Fig. 9c).

Table 2
The *d*-spacings (nm) between PEG-rich domains as obtained from room temperature SAXS data.

Non-iodinated polymers				Iodinated polymers			
PEG content		*d*-spacings		PEG content		*d*-spacings	
Mol%	wt%	dry	wet	Mol%	wt%	dry	wet
0%	0			0%	0.0		
5% PEG_{1k}	12.8			5% PEG_{1k}	9.8		
8% PEG_{1k}	19.6		13.4	8% PEG_{1k}	12.5		
10% PEG_{1k}	23.7		12.6	10% PEG_{1k}	15.4		19.6
20% PEG_{1k}	41.2		16.4	24% PEG_{1k}	34.1		12.3
15% PEG_{2k}	49.7	22.4[a]	14.5	15% PEG_{2k}	36.7		12.0
30% PEG_{2k}	70.6	14.8	14.2	30% PEG_{2k}	58.5	18.0	9.4
0.71% PEG_{35k}	41.2	17[a]	22.4	8% $PEG_{8k\ 8k}$	53.3	19.0	22.9
PLLA	0	23.3	27.3				

[a] Weak shoulder.

a random coil of PEG_{8k} [46]. The length of a rod-like PEG_{1k} block with helical chains is ~7 nm [47]. Therefore, the observed 10 nm-size hydrated domains are formed as a few PEG segments, perhaps with an occasional DTE segment, come together and trap water molecules that are hydrogen-bonded to the polymer chains in the PEG-rich phase. These ideas are illustrated in Fig. 7b.

The changes observed in the SAXS patterns (Fig. 6) as the sample was heated through the melting point of ice can be explained using a 1D model (Fig. 7c). The electron density of water, amorphous PEG, and DTE are 334, 369, and 412 nm^{-3}, respectively. Thus, there is some electron density contrast between PEG and the DTE matrix when the sample is dry, and this contrast is enhanced when the PEG blocks are hydrated. At $T > 0$ °C, PEG–water hydrogen-bonding interactions result in microphase separation of PEG-rich domains and thus give rise to periodic fluctuations in electron density that result in an intense SAXS peak. At $T < 0$ °C, when water is frozen and has phase separated into ice crystals, the absence of water-mediated hydrogen-bonding and the concomitant redistribution of the adjacent PEG chains reduces fluctuations in electron density along the chain. As a result, the SAXS peak is not expected in frozen, high-PEG polymers. This model applies equally well to the iodinated polymers. The electron density remains uniform along the main chain when water crystallizes into ice causing PEG segments to de-segregate, and the SAXS peaks will be more intense when the PEG domains are ordered, which was indeed observed.

3.6. Melting of PEG–ice complex

Fig. 8a shows an example of the changes in the intensity of the 101 reflection of ice in the WAXS scans (Fig. 5a) during heating and cooling of a PEG–DTE copolymer. This figure illustrates the large hysteresis in the melting and the crystallization of ice [48]. During cooling, the intensity of the ice crystalline peaks begins to increase at −10 °C and reach a plateau at −20 °C. During heating, the intensity decreases gradually from −40° to ~0 °C, and disappears between 0 and 10 °C. Although the X-ray data were collected with the sample pan vertical in the Linkham unit, it is not likely that this hysteresis is due to poor thermal contact between the pan and heater plate because the same hysteresis is seen in the DSC scans (Fig. 8b; 15% PEG_{2k}) that were obtained on a Mettler unit where the sample pan was horizontal. At heating rates typically used in DSC scans (10 °C/min), free water shows a broad melting peak that starts at 0 °C and is centered at ~5 °C. At cooling rates of 10 °C/min used in this study, which are typical, the free water supercools and freezes at ~−20 °C [11,49]. Such sharp freezing exotherm and broad melting behavior for water was seen in all of our samples with at least ~1 wt% water. Similar transitions have been reported for lipid layers [48].

The effect of hysteresis in the melting of ice manifests in the SAXS data associated with the self-assembled phase separated domains (Fig. 8c). Upon cooling, the intensity of the SAXS peak begins to decrease at −10 °C as the ice begins to crystallize, and disappears as soon as the crystallization of ice is complete. Upon heating the polymer through the melting transition of ice, the SAXS peak begins to increase before the ice melts. This increase occurs over a much broader temperature range from −20 °C to 20 °C, and reaches a plateau by the time all the ice has melted. The appearance

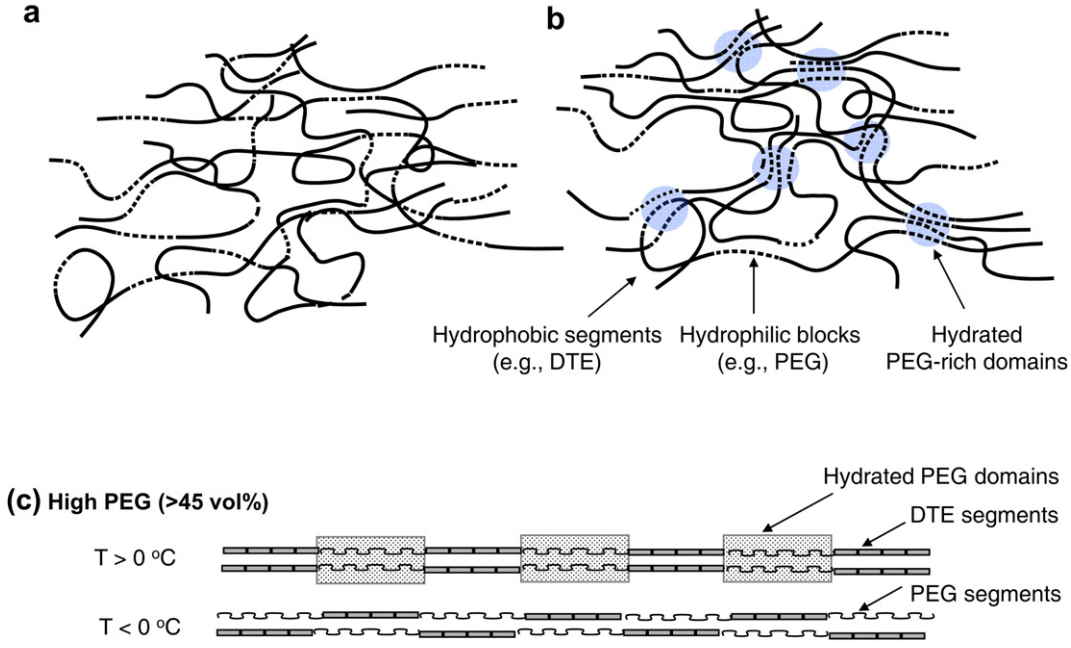

Fig. 7. Schematic representations of the proposed arrangements of PEG and DTE segments. (a) Uniform distribution in dry samples. (b) PEG-rich domains in hydrated samples. (c) Reversible changes in segregation of PEG domains during melting of ice and freezing of water. High electron density regions due to the overlap of the PEG segments are shown as shaded blocks. The average electron density is periodic when water is present and is uniform when it is frozen.

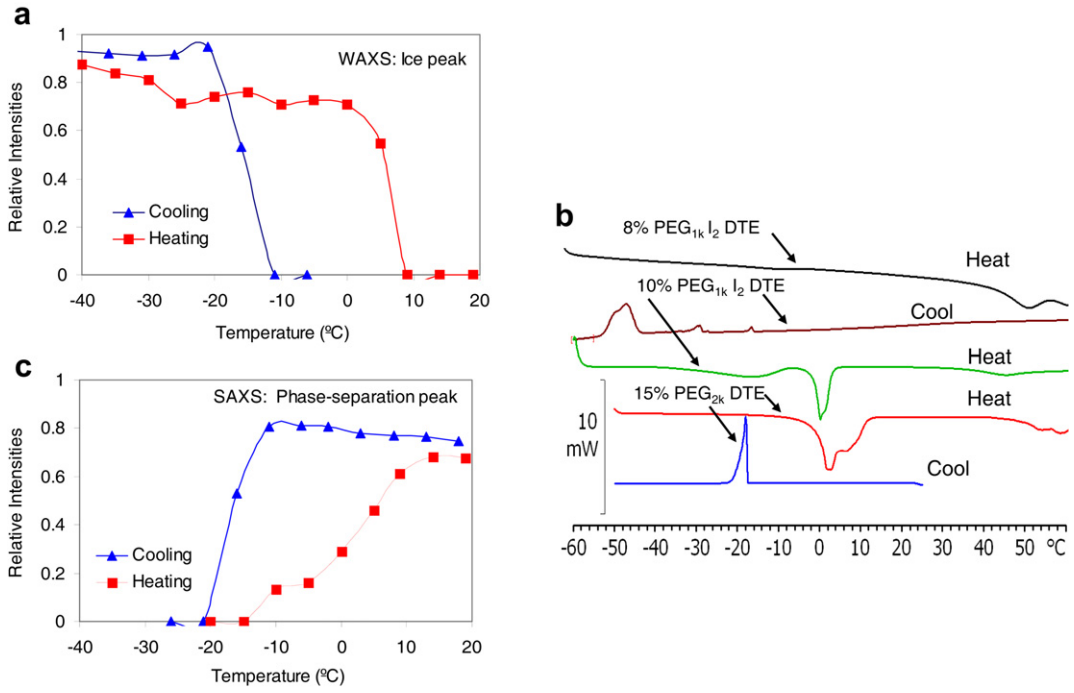

Fig. 8. (a) Plot of the changes in the intensity of 101 reflection ($q \sim 18$ nm^{-1}) of the hexagonal ice (WAXS), during heating (red squares) and cooling (blue triangles) of 15% PEG_{2k} DTE. (b) DSC scans showing the transitions near the melting point of ice. Scans from top to bottom: 8% PEG_{1k} I_2DTE shows no crystallizable water; 10% PEG_{1k} I_2DTE that shows a eutectic of PEG and water; 15% PEG_{2k} DTE that shows bound water melting at ~10 °C along with the melting of free water; typical freezing of liquid (free) water upon cooling as seen in the 15% PEG_{2k} DTE. (c) Intensity of the SAXS interference peak in a 15% PEG_{2k} DTE during heating (red squares) and cooling (blue triangles). (For interpretation of the references to colour in this figure legend, the reader is referred to the web version of this article).

of a SAXS peak during the heating segment when ice is still present (Fig. 8c and a), shows that the SAXS peak is not a result of the changes in the contrast due to the changes in the state of water. The segregated amorphous PEG domain by itself has enough contrast in the DTE matrix, and water or ice simply enhances this contrast. Thus, the changes in the SAXS are due to the phase separation of PEG segments from the DTE matrix.

The WAXS data show that the ice crystals disappear over a narrow temperature range. In contrast, changes occur over a broader temperature range in SAXS, and are indicative of the slower diffusion of water into PEG-rich regions that is determined both by temperature- and time-dependent processes. Most importantly, the data show that the state of water, not just its presence, determines the phase behavior; water and the polymer chains need to be mobile for the phase separation to occur.

The melting and freezing behaviors of water in polymer systems are sensitive to the thermal history and are quite complex [50–52]. Therefore, a detailed study of the behavior and transformation between these states is beyond the scope of this study. Instead, some of the interesting features in the freezing and melting behavior of water observed in DSC and WAXS scans in our polymers will be identified. At least three types of melting behavior, some examples of which are shown in Figs. 8b and 9a, were observed as the frozen samples were heated in the DSC: (1) a broad melting peak at $T > 0$ °C (10% PEG_{1k} I_2DTE-heat; Fig. 8b) typical of free water, and in some cases complete melting of bound water at 10 °C (15% PEG_{2k} DTE-heat; Fig. 8b) that was confirmed by WAXS data (Fig. 8a); (2) a sharp melting peak at 0 °C (Fig. 9a); and (3) a broad melting peak below 0 °C (Fig. 8a and 10% PEG_{1k} I_2DTE-heat) attributed to PEG–water eutectic [53–58]. Some of these peaks overlap, and similar multiple melting peaks have been reported in other PEG-containing polymers [11]. Upon cooling, in most samples, water was found to freeze at −20 °C (Fig. 8b and 15% PEG_{2k} DTE-cool and Fig. 9a-cool) [56]. Some samples could be supercooled to −40 °C before water crystallized (Fig. 8b and 10% PEG_{1k} I_2DTE-cool and Fig. 9a-cool), and this is usually attributed to an eutectic of water and PEG [55,58]. Finally, water is also present in a non-freezable bound form [50,59,60] in low-PEG polymers, as seen by the absence of a melting peak of ice (e.g., Fig. 8b, 8% PEG_{1k} I_2DTE-heat) although they contained up to 6 wt% water. These low-PEG polymers did not show any phase separation of PEG-rich hydrated domains in SAXS data. These melting and freezing behaviors suggest that water in the copolymer is present as free and bound water, the latter in both freezing and non-freezing forms [60,61].

3.7. Structural transition between 20 and 70 °C

The structural changes that occur after the ice was melted were highly dependent on the composition of the copolymer. The DSC scan in Fig. 9a, typical of the low-PEG (8 and 10% PEG_{1k}) polymers, shows enthalpic relaxations between 40 and 60 °C during the first heat and not during the second-heat. These were accompanied by irreversible changes in the morphology indicated by changes in the 19 nm^{-1} shoulder in the WAXS of the 10% PEG_{1k} DTE polymer (Fig. 9b). This shoulder is weak during the first heat, disappears above 30 °C, and does not reappear upon cooling, even though presence of water is evident in the crystalline ice peaks at −20 °C. The SAXS peak with a d-spacing of 12.6 nm that disappeared upon heating ($q = 0.5$ nm^{-1}, Fig. 6b) appeared as a different peak with a d-spacing of 21 nm ($q = 0.3$ nm^{-1}, Fig. 9c) upon cooling. The new morphologies in the once-heated samples were reversible during subsequent heat and cool cycles as seen in both the SAXS and WAXS patterns. These changes were not accompanied by molecular weight degradation as confirmed by GPC (in dimethyl formamide) measurements of compression-molded films after hydration. Since

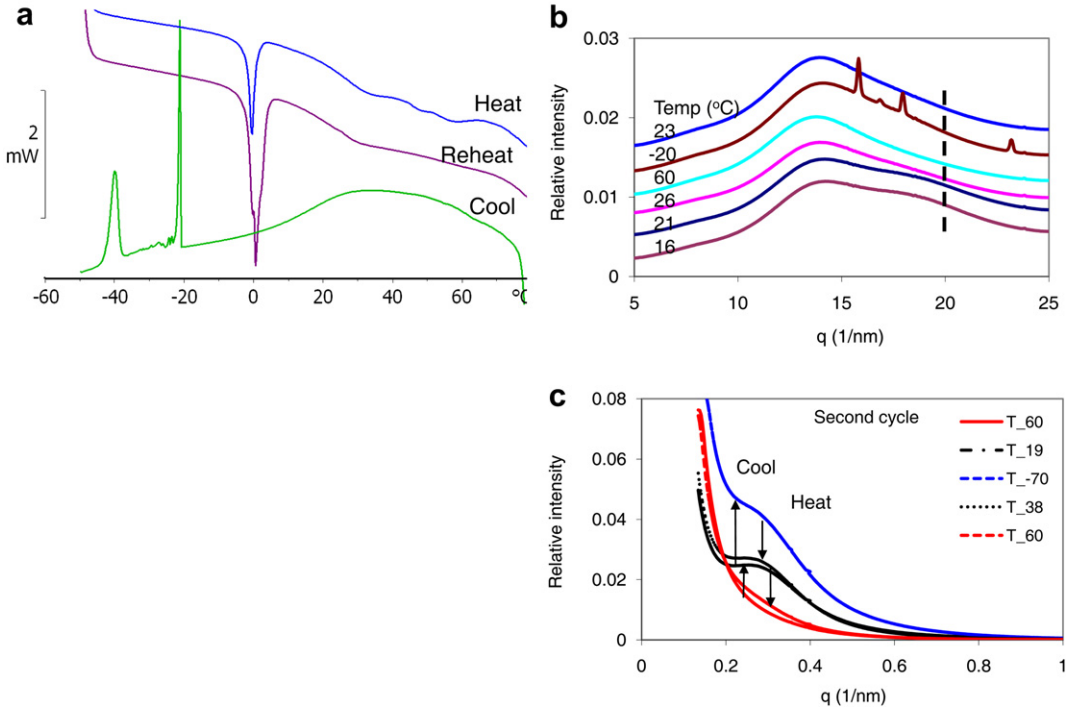

Fig. 9. DSC, WAXS and SAXS data from the 10 mol% PEG–DTE copolymer showing irreversible transitions between 20 and 60 °C. (a) DSC data showing the irreversible transitions between 40 and 60 °C during heating, and the −40 °C crystallization endotherm along with the crystallization of ice during cooling. (b) WAXS scans showing the disappearance of the 19 nm^{-1} water shoulder at $T > 26$ °C, and non-reappearance upon reheating. (c) SAXS scans of the sample used in Fig. 6b but now shown during the second heating cycle. The scans in (a) and (b) have been vertically offset for clarity.

PEG melts between 40 and 60 °C, and because similar transitions occur in hydrated PEG (unpublished), the transitions between 40 and 60 °C can be attributed to relaxations and the accompanying changes in the organization of the PEG segments. The appearance of the supercooled crystallization peak at −40 °C (Fig. 9a), which was invariably seen during the second cooling cycle and usually attributed to PEG–water eutectic, is indicative of the reorganization of the PEG–water complex.

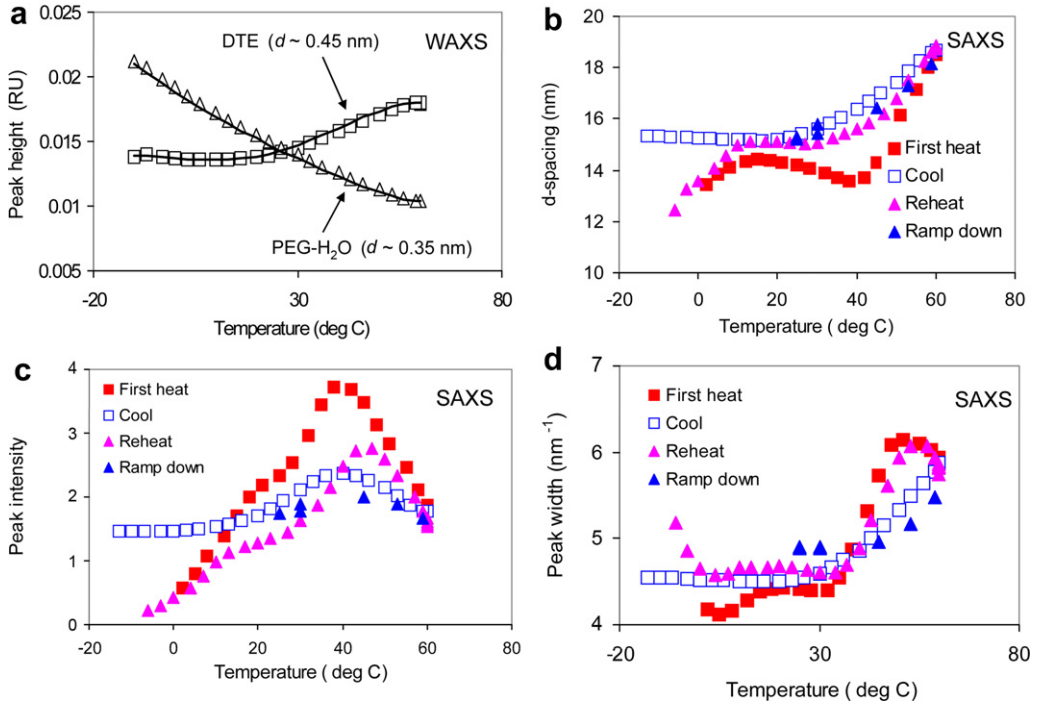

Fig. 10. Reversibility of the structure with temperature in the wet 20% PEG_{1k} DTE. (a) Intensity of the DTE ($q = 14$ nm^{-1}, $d = 0.45$ nm) and the PEG–water ($q = 19$ nm^{-1}, $d = 0.35$ nm) peaks seen in WAXS. The data obtained during cooling runs are plotted to show the values below the freezing point of water. (b) SAXS d-spacings. (c) SAXS intensity (d) SAXS peak width.

Much larger changes were observed with temperature in high-PEG polymers both with and without iodine as illustrated in Fig. 10, based on data from 20% PEG_{1k} DTE. The WAXS scan in Fig. 10a shows that as the temperature increases from 15 °C, the intensity of the hydrated PEG peak (Fig. 5a, $q = 19\ nm^{-1}$) decreases, and from 45 to 60 °C, the intensity of the DTE peak (Fig. 5a, $q = 14\ nm^{-1}$) increases. This pattern was reversed during cooling (data not shown): the decrease in the intensity of the DTE peak was accompanied by an increase in the intensity of the hydrated PEG peak until water froze at −20 °C. The SAXS profiles demonstrate additional temperature-induced effects (Fig. 10b–d): The distance between PEG domains increases, the interference peak intensity first increases and then begins to decrease, and the peak-width (a measure of the degree of coherence between the domains: the larger the width the smaller the degree of correlation) increases. Onset of the redistribution of PEG from PEG-rich domains into the rest of polymer could reduce the electron density contrast and thus account for the large changes in SAXS intensity at 37 °C and other parameters in the SAXS data. Such redistribution of PEG can also account for the decrease in the intensity of the hydrated PEG peak and the increase in that of the DTE peak in the WAXS data. This model also suggests that the PEG domains, which absorb water quickly, act as reservoirs from which water diffuses more slowly into the hydrolyzable segments of the polymer. Some of the changes in the SAXS curves at ~40 °C that are clearly seen in Fig. 10b and c occur only during the first heat and not during subsequent cooling and heating. Similar irreversible changes are also apparent in the DSC, WAXS and SAXS scans shown in Fig. 9.

4. Conclusions

Simultaneous SAXS/WAXS/DSC studies from a family of random segmented copolymers of PEG and DTE polymers provide results that are generally useful for understanding the temperature- and hydration-induced structural changes at molecular length scale (1 nm) and the phase behavior at mesoscales (10 nm) in polymers with hydrophilic and hydrophobic blocks.

In the polymers exposed to water, PEG–water eutectics were observed in the DSC scans, diffraction peaks ($d = 0.35$ nm) due to PEG–water complexes were observed in WAXS patterns, and clusters of hydrated PEG domains ($d \sim 15$ nm) were observed in SAXS in polymers with >15 vol% PEG (3 wt% water). These hydrated domains are thought to be the precursors for the formation of interconnected water channels that facilitate polymer erosion and drug release.

When the polymer is dry, more than ~50 vol% PEG is required for PEG blocks to crystallize. It is important to be cautious in studying the phase behavior with SAXS. In iodinated polymers with >70 vol% PEG, at all temperatures, a SAXS interference peak was observed. This peak is attributed to clusters or ordered hydrophilic, phase-separated PEG domains in the hydrophobic DTE matrix. The same peak was observed in non-iodinated polymers but only above the T_g. This is best explained by the lack of electron density contrast between crystalline PEG and glassy, non-iodinated DTE segments below the T_g of the copolymer.

Phase behavior of the hydrated copolymer was dependent on the PEG content: the PEG-rich domains formed clusters both below and above 0 °C at low PEG contents, and only after the ice had melted at high PEG contents. Secondary melting transitions between 20 and 70 °C, and the accompanying structural changes at ~40 °C could be of significance in understanding the behavior of these materials in biomedical devices.

Acknowledgement

We thank D. Lewitus, A. Luk, D. Grubb and H. Koerner for their comments on the manuscript. This work was supported by RESBIO (Integrated Technology Resource for Polymeric Biomaterials) funded by National Institutes of Health (NIBIB and NCMHD) under grant P41 EB001046. The content is solely the responsibility of the authors and does not necessarily represent the official views of the NIH, NIBIB or NCMHD. The work was also funded by NSF grant DMR-0735242 and by the New Jersey Center for Biomaterials. The X-ray scattering work was carried out at the Advanced Photon Source (APS), Argonne National Laboratory, which is funded by DOE, and we thank Dr. Steven Weigand at the APS for enabling us to obtain the X-ray data. We thank Ilya Grinberg for assistance with DSC.

References

[1] Guo S, Shen L, Feng L. Polymer 2001;42:1017–22.
[2] Abuchowski A, van Es T, Palczuk NC, Davis FF. J Biol Chem 1977;252:3578–81.
[3] Merrill EW. Poly(ethylene oxide) and blood contact. In: Harris JM, editor. Poly (ethylene glycol) chemistry biotechnical and biomedical applications. New York and London: Plenum Press; 1992.
[4] Cohn D, Hotovely-Salomon A. Polymer 2005;46:2068–75.
[5] Lisowski MS, Liu Q, Cho J, Runt J, Yeh F, Hsiao BS. Macromolecules 2000;33: 4842–9.
[6] Ito H, Russell TP, Wignall GD. Macromolecules 1987;20:2213–20.
[7] Inomata K, Nakanishi E, Sakane Y, Koike M, Nose T. J Polym Sci Polym Phys 2005;43:79–86.
[8] Sun L, Liu Y, Zhu L, Hsiao BS, Avila-Orta CA. Polymer 2004;45:8181–93.
[9] Sun L, Liu Y, Zhu L, Hsiao BS, Avila-Orta CA. Macromol Rapid Commun 2004;25:853–7.
[10] Mai S-M, Patrick J, Fairclough A, Terrill Nicholas J, Turner SC, Hamley IW, et al. Macromolecules 1998;31:8110–6.
[11] Husken D, Gaymans RJ. Macromol Chem Phys 2008;209:967–79.
[12] Maiti S, Chatterji PR, Nisha CK, Manorama SV, Aswal VK, Goyalz PS. J Colloid Interface Sci 2001;240:630–5.
[13] Fairclough JPA, Norman AI, Shaw B, Nace VM, Heenan RK. 2006;55:793–7.
[14] Lin Y, Alexandridis P. J Phys Chem 2002;106:12124–32.
[15] Agrawal SK, Sanabria-DeLong N, Jemian PR, Tew GN, Bhatia SR. Langmuir 2007;23(9):5039–44.
[16] Deschamps AA, Grijpma DW, Feijen J. J Biomater Sci Polym Ed 2002;13 (12):1337–52.
[17] van Dijkhuizen-Radersma R, Roosma JR, Kaim P, Metairie S, Peters FL, de Wijn J, et al. J Biomed Mater Res A 2003;67(4):1294–304.
[18] Leibler L. Macromolecules 1980;13:1602–17.
[19] Bates FS, Schulz MF, Khandpur AK, Förster S, Rosedale JH, Almdal K, et al. Faraday Discuss 1994;98:7–18.
[20] Bates FS. Science 1991;251:898–905.
[21] Mortensen K, Almdal K, Schwahn D, Bates FS. J Appl Crystallogr 1997;30:702–7.
[22] Ruzette A-V, Leibler L. Nat Mater 2005;4:19–31.
[23] Hadjichristidis N, Pispas S, Floudas GA. Block copolymers: synthetic strategies, physical properties and applications. Chichester, UK: John Wiley & Sons, Ltd; 2002.
[24] Abetz V, Simon PFW. Phase behaviour and morphologies of block copolymers. In: Abetz V, editor. Advances in polymer Science- block copolymers I, vol. 189. Springer; 2005. p. 125–212.
[25] Hamley IW. The physics of block copolymers. Oxford University Press; 1999.
[26] Hamley IW. Developments in block copolymer science and technology. Wiley; 2004.
[27] Muller AJ, Balsamo V, Arnal ML. Nucleation and crystallization in diblock and triblock copolymers. In: Abetz V, editor. Adv polym sci–block copolymers II, vol. 190. Berlin Heidelberg: Springer; 2005. p. 1–63.
[28] Santoveña A, Alvarez-Lorenzo C, Concheiro A, Llabrés M, Fariña JB. J Biomater Sci Polym Ed 2005;16:629–41.
[29] Tew GN, Sanabria-DeLong N, Agrawal SK, Bhatia SR. Soft Matter 2005;1:253–8.
[30] Dorati R, Genta I, Colonna C, Modena T, Pavanetto F, Perugini P, et al. Polym Degrad Stabil 2007;92:1660–8.
[31] Deng XM, Xiong CD, Cheng LM, Huang HH, Xu RP. J Appl Polym Sci 1995;55 (8):1193–6.
[32] Deschamps AA, van Apeldoorn AA, Hayen H, de Bruijn JD, Karst U, Grijpma DW, et al. Biomaterials 2004;25(2):247–58.
[33] Kohn JB, Bolikal D, Pendharkar SM. US Patent: 7056493; 2006.
[34] Pendharkar SM, James K, Kohn J. Soc Biomater 1998;21:386.
[35] Yu C, Kohn J. Biomaterials 1999;20:253–64.
[36] Kohn J, Zeltinger J. Expert Rev Med Devices 2005;2(6):667–71.
[37] Khan IJ, Murthy NS, Kohn J. ACS Polym Preprints 2009;(2).
[38] Hammersley AP, Svensson SO, Thompson A, Graafsma H, Kvick Å, Moy JP. Rev Sci Instrum 1995;66:2729–33 (SRI-94).
[39] Li CY, Birnkrant MJ, Natarajan LV, Tondigli VP, Lloyd PF, Sutherland RL, et al. Soft Matter 2005;1:238–42.
[40] Bedoui F, Widjaja LK, Luk A, Bolikal D, Murthy NS, Kohn J. In: Narayan R, editor. Enhancement of mechanical properties upon hydration in copolymers of PEG and iodinated tyrosine-derived polycarbonates. MRS; 2009.

[41] Mark PR, Murthy NS, Weigand S, Breitenkamp K, Kade M, Emrick T. Polymer 2008;49:3116–24.
[42] Hamley IW, Fairclough JPA, Ryan AJ, Mai SM, Booth C. Phys Chem Chem Phys 1999;1:2097–101.
[43] Stewart GW. Physiol Rev 1931;37:9–16.
[44] Murthy NS, Orts WJ. J Polym Sci Poly Phys 1994;32:2695–703.
[45] Sousa A, Schut J, Kohn J, Libera M. Macromolecules 2006;39(21):7306–12.
[46] Murthy NS, Braswell EH, Knox JR. Biopolymers 1988;27:865–81.
[47] Takahashi Y, Tadokoro H. Macromolecules 1973;6(5):672–5.
[48] Gleeson JT, Erramilli S, Gruner SM. Biophys J 1994;67:706–12.
[49] Wilson PW, Arthur JW, Haymet ADJ. Biophys J 1999;77:2850–5.
[50] Ohno H, Shibayama M, Tsuchida E. Makromol Chem 1983;184:1017–24.
[51] Sartor G, Mayer E. Biophys J 1994;67:1724–32.
[52] Ehre D, Lavert E, Lahav M, Lubomirsky I. Science 2010;327:672–5.
[53] Hager SL, Macrury TB. J App Polym Sci 1980;25:1559–71.
[54] Hey MJ, Nett SM. J Chem Soc Faraday Trans 1991;87:3671–5.
[55] Huang L, Nishinari K. J Polym Sci Part B Polym Phys 2001;39:496–506.
[56] Vringer Td, Joosten JGH, Junginger HE. Colloid Polym Sci 1986;264:623–30.
[57] Bogdanov B, Mihailov M. J Polym Sci Part B Polym Phys 1985;23:2149–58.
[58] Graham NB, Zulfiqar M, Nwachuku NE, Rashid A. Polymer 1989;30:528–33.
[59] Varma-Nair M, Costello CA, Colle KS, King HE. J Appl Polym Sci 2007;103:2642–53.
[60] Zhang J, Teng H, Zhou X, Shen D. Polym Bull 2002;48:277–82.
[61] Meakin JR, Hukins DWL, Imrie CT, Aspden RM. J Mater Sci Mater Med 2003;14:9–15.